CrossMark

INVITED ARTICLE

High-temperature stable single carrier hole only device based on conjugated polymers

Shahidul Alam[a)]
Center for Energy and Environmental Chemistry Jena (CEEC Jena), Friedrich Schiller University Jena, Jena 07743, Germany; and Laboratory of Organic and Macromolecular Chemistry (IOMC), Friedrich Schiller University Jena, Jena 07743, Germany

Peter Fischer
Institute of Materials Engineering, Technische Universität Ilmenau, Ilmenau 98693, Germany

Christian Kästner
Institute of Thermodynamics and Fluid Mechanics, Technische Universität Ilmenau, Ilmenau 98693, Germany

Chetan R. Singh
Department of Macromolecular Chemistry I, University of Bayreuth, Bayreuth D-95440, Germany

Ulrich S. Schubert and Harald Hoppe[b)]
Center for Energy and Environmental Chemistry Jena (CEEC Jena), Friedrich Schiller University Jena, Jena 07743, Germany; and Laboratory of Organic and Macromolecular Chemistry (IOMC), Friedrich Schiller University Jena, Jena 07743, Germany

(Received 15 January 2018; accepted 1 June 2018)

Thin hole transport layers are important elements in organic semiconductor-based devices. Metal oxides are an encouraging material class for this purpose, as they may provide sufficient hole conduction in combination with excellent electron blocking properties. Both, long-term device stability, which may often be limited by the thermal stability of interfaces, and higher temperature processing steps, benefit strongly from the existence of thermally stable metal oxide interlayers. Provided that thermally stable electrodes can be fashioned, the stability of organic active layers—for example, in organic field effect transistors, light emitting diodes, or photovoltaic (OPV) devices can be investigated. Here, we apply this concept and report about the study of hole mobility (μ_h) in single-carrier-hole-only devices in dependence of thermal annealing up to the above the actual melting temperature of regio-regular poly(3-hexylthiophene-2,5-diyl) (P3HT).

I. INTRODUCTION

The structural order of conjugated polymers and organic molecules, in terms of conformation, aggregation/crystallization, and spatial organization, has a tremendous impact on charge transport properties in organic semiconductor devices.[1–3] As a consequence, the film deposition method itself may introduce strong anisotropies in semiconductor organization and thus alongside with that charge transport may exhibit a high orientational dependency. Controlling factors of the molecular organization during the film formation process are OSC material properties (e.g., M_N, M_W, and PDI for polymers), choice of solvent and solution concentration, preconditioning in solution, and deposition method, as well as processing temperature and atmosphere during deposition. Thus various properties such as molecular aggregation and crystallinity, as well as anisotropy can be fine-tuned by balancing cohesion and adhesion forces.[4–7]

While it is known that the charge carrier density may play a crucial role in charge carrier mobility,[8] and thus highest mobility can generally be obtained for lateral geometry in organic field-effect transistors by making use of mobility anisotropy,[9] the function of organic solar cells essentially depends on the vertical charge transport capabilities. Hence, evaluating the charge carrier mobility of OSCs for use in organic solar cells requires the application of time-of-flight, charge-extraction-by-linearly-increasing-voltage, or space-charge-limited-current (SCLC) methods. The advantage of the latter approach allows investigation of film thicknesses of close to those commonly used in organic photovoltaic devices.[10–12]

Furthermore, not only the processing of organic solar cells may require the application of thermal annealing steps but also an investigation of photoactive layer stability involves the use of increasing thermal stress recently.[13,14] As a long-term, smaller thermal stress may accumulate to a correspondingly shorter but higher thermal stress; the photovoltaic layer stack should not

Address all correspondence to these authors.
[a)]e-mail: shahidul.alam@uni-jena.de
[b)]e-mail: harald.hoppe@uni-jena.de
DOI: 10.1557/jmr.2018.203

 © Materials Research Society 2018

https://doi.org/10.1557/jmr.2018.203 Published online by Cambridge University Press

limit the thermal stability of such devices itself. Ultimately, the charge carrier mobility (μ) of semicrystalline semiconductors such as P3HT can be optimized by melt-crystallization[15] or a combination of melt-crystallization and orientation of P3HT-backbones vertically to the substrate.[16–20] Thus, the quest for thermally stable layer stacks and charge extraction layers gained importance for further developing OPV stability and the search for performance limitations. In this contribution, we focused on the thermal stability of the hole extraction layer–electrode combination. By application of single-carrier hole-only SCLC diode devices, superior stability of molybdenum oxide (MoO_3)/gold (Au) is demonstrated, which is sufficient to evaluate melt crystallization of the semicrystalline polymer P3HT. It should be noted that the test is performed in the injection mode. However, superior injection as required for obtaining the space-charge-limit is requiring ohmic contacts and thus as well efficient extraction of charge carriers across the same electrode can be concluded.

II. EXPERIMENTAL

The nominal energy levels according to the literature of the materials used in this study, and an exemplary SCLC device architecture and the chemical structure of P3HT are shown in Figs. 1(a)–1(c), respectively. The P3HT batch (P200) used in this study was purchased from BASF. The polymer was dissolved in chlorobenzene yielding solutions of 2 wt% (20 mg/mL). The solutions were prepared and stored in the glovebox under a nitrogen atmosphere at 50 °C and continuously stirred at 600 rpm for at least two weeks.

The hole transport layers (HTLs) used in this study were either poly(3,4-ethylenedioxythiophene)-poly(styrene sulfonate) (PEDOT:PSS) (formulation Heraeus Clevios PH) or MoO_3, both in contact with gold electrodes. PEDOT:PSS (was modified by the addition of 10 vol% Isopropanol) and the formulation was spin cast in all cases outside of the glovebox at 3000 rpm, no matter at which side it was used. PEDOT:PSS films were always annealed at 178 °C for 15 min for drying. In the case where PEDOT:PSS was applied on top of the P3HT layers, this already yielded some annealing of the P3HT layer. MoO_3 and gold were deposited by physical vapor deposition within a glovebox-attached MiniSpectros from Kurt J. Lesker (Jefferson Hills, Pennsylvania). All films, layer stacks, and complete devices were processed on top of float glass.

A. Film, layer stack, and hole-only SCLC device preparation

Single-carrier hole-only SCLC devices were prepared on glass substrates, yielding a device area of 4 mm^2 via the definition of gold electrode overlap. Two different sets of devices were realized: asymmetric devices, bearing on one of the two sides only gold as an injection or extracting electrode, and symmetric devices, were on both sides either PEDOT:PSS or MoO_3 was used as a modification of the gold electrodes. The sample preparation consisted of substrate cleaning and deposition of gold, HTLs (MoO_3 and PEDOT:PSS) and P3HT active layer on the substrates. Bare glass substrates were subsequently cleaned with acetone and isopropanol in an ultrasonic bath and dried via N_2 gun. 100 nm of Au was thermally evaporated on cleaned substrates under high vacuum conditions from tungsten boat; the evaporation rate was 20 A/s. The

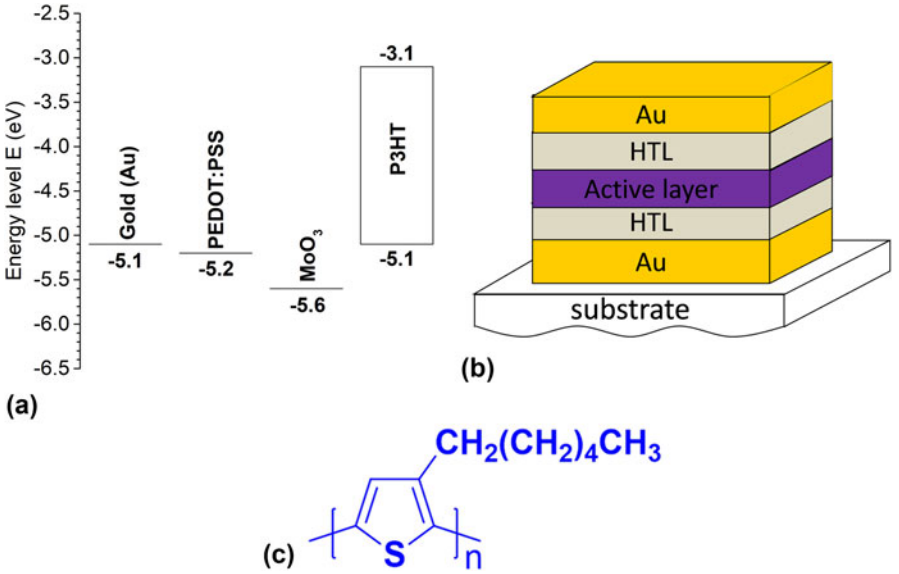


FIG. 1. Energy level diagram of the materials are used in the studies[21,22] (a), an exemplary SCLC device architecture (b), and the chemical formula of regio-regular P3HT (c) are depicted.

https://doi.org/10.1557/jmr.2018.203 Published online by Cambridge University Press

electrode structure was defined by the shadow mask that was used for the evaporation. After that, either no HTL, 30 nm of PEDOT:PSS or 15 nm MoO_3 were deposited by either spin coating or thermal evaporation (physical vapor deposition) through a shadow mask, respectively. The evaporation rate for MoO_3 was 8 A/s. Then a ~300 nm thick layer of P3HT was spin cast on top; the spin coating process was performed inside the glovebox. Finally, either no HTL, PEDOT:PSS or MoO_3 was deposited over the P3HT active layer, or yielding either asymmetric or symmetric devices. Devices were completed with the thermal evaporation of the gold top electrode through shadow mask exactitude an active area of 0.04 cm^2. SCLC devices were subjected to thermal annealing between 150 and 250 °C with 50 °C increments for 10 min. To protect the completed devices from environmental conditions, the samples were encapsulated using glass and an UV-curing epoxy resin under an inert environment. An exemplary layer stack of the device is depicted in Fig. 1(b).

B. SCLC device characterization

The SCLC devices were characterized in the dark at room temperature with a computer-controlled Keithley 2400 source measure unit (Keithley Instruments, Solon, Ohio). Dark *I–V* data were recorded from −8 to +8 V. To evaluate the charge carrier mobility, the *I–V* curves were fitted by using the Murgatroyd SCLC formula for the mobility (μ_h) determination.[23] Thereby a slight variation of the built-in voltage (V_{bi}) was allowed and evaluated via best fit. The series resistances of specific electrode structures were determined from the respective reference devices fabricated without the active layer.

C. Atomic force microscopy

Film topography was characterized with a Veeco/Bruker Dimension atomic force microscopy (AFM; Veeco Instrument Co., Bruker, Plainview, New York) in the tapping mode, to gain further insight into possible changes of charge transport layers, using super sharp tips (TESP-SS). The images were analyzed by Nanoscope v720 software (Bruker, Karlsruhe, Germany). For AFM measurements, either PEDOT:PSS or MoO_3 on gold were investigated.

D. Kelvin probe

To detect a possible change in work function of the layers upon annealing, a single point Kelvin probe (KP) system from Anfatec was used. The probe head dimension was 1.4 mm^2. For calibration of the system, freshly cleaved highly oriented pyrolytic graphite was used, and work functions were calculated based on the difference measured.

III. RESULTS AND DISCUSSION

In SCLC devices, the current–voltage (*I–V*) characteristics are controlled by two fundamental processes: first, injection of charge carriers from the electrodes into the active layer and extraction from the same into the second electrode, second, charge transport in the bulk of the active layer. Thus, the current is either injection (ILC) or bulk limited via built-up of a space charge region. The latter condition is desired in SCLC devices, to determine the charge carrier mobility within the OSC, in this case, P3HT, which was subjected to various annealing conditions. Thus, it is mandatory to have optimized ohmic contacts to ensure that injection is not limiting and hence the electrode-HTL combinations are yielding the highest overall current densities and associated with the hole mobilities also depict optimal interfacial contacts in case of solar cells.

Since OSCs are intrinsically disordered, charge carriers transport happens under the presence of potential barriers causes electric field dependence on charge carrier mobility. This generally is determined by the Poole–Frenkel mobility determination model $\mu = \mu_0 \exp\left(\gamma\sqrt{E}\right)$, where μ_0 represents the zero electric field and γ is the electric field enhancement factor.

Thus current–voltage (*I–V*) measurements have been performed to determine the best choice of HTL. Governed by conductivity via intrinsic charge carriers (e.g., due to doping), the *I–V* characteristics are mostly linear at low bias voltages and become superliner at higher voltages. In case of trap-free charge transport, the slope of the curve at higher voltage becomes 2, according to the Child's law. In smaller deviations, these exponents are possible due to electric field enhancements, as described by the Poole–Frenkel model. Taking this effect into account leads to the application of the Murgatroyd SCLC formula:

$$J = 9/8\varepsilon\varepsilon_0\mu_h \exp\left(0.89\gamma\sqrt{F}\right)V^2L^{-3} \quad , \qquad (1)$$

where J is the hole current density, μ_h is the zero field mobility of holes, ε is the relative permittivity of the material (3.5), ε_0 is the permittivity of the vacuum, γ is the field activation factor, L is the thickness of the active layer, and $F = V/L$ is the average electric field across the device. The SCLC hole mobility (μ_h) of P3HT was determined on devices annealed under different temperatures. Table I summarizes the variation in the bottom and top HTLs of the different SCLC devices realized.

Figure 2 depicts the *J–V* characteristics of the devices with asymmetric contact materials from as-cast up to annealing temperatures of 250 °C. Most devices actually exhibit asymmetric characteristics, when comparing the forward and reverse currents. Only in case of the Au/P3HT/PEDOT:PSS/Au devices, all curves fall on top of each other and show symmetric behavior with respect to the sign of voltage applied.

As devices exhibiting MoO_3 HTLs demonstrated already higher current densities, the deviation is not

https://doi.org/10.1557/jmr.2018.203 Published online by Cambridge University Press

likely to stem from bulk charge transport. Thus all asymmetric devices displaying PEDOT:PSS on either side of the P3HT active layer do not seem to show the actual hole mobility and must be injection limited. However, it remains not fully understood why forward/reverse currents of the Au/PEDOT:PSS/P3HT/Au device does not reproduce the reverse/forward currents of the Au/P3HT/PEDOT:PSS/Au device. At this point, it can only be concluded that the interfacial property of the PEDOT:PSS injection layer depends on the order of processing, or in other words, PEDOT:PSS exhibits a different interfacial organization when processed on top instead of below the P3HT layer. This can be in part comprehended, as it has been shown earlier that commonly the PSS groups are enriched at the surface of any PEDOT:PSS layer and furthermore facilitate improved injection via interfacial doping[24] and also interface dipoles are possible.

TABLE I. Overview of the experimental variation of HTLs.

Bottom electrode	Bottom HTL	Active layer	Top HTL	Top electrode
Gold	PEDOT:PSS	P3HT	x	Gold
Gold	x	P3HT	PEDOT:PSS	Gold
Gold	MoO_3	P3HT	x	Gold
Gold	x	P3HT	MoO_3	Gold
Gold	PEDOT:PSS	P3HT	PEDOT:PSS	Gold
Gold	MoO_3	P3HT	MoO_3	Gold

The presence of PSS at the interface may further explain the degradation of injection properties for temperatures above 150 °C for the Au/PEDOT:PSS/P3HT/Au layer stack. As already stated, devices containing one MoO_3 HTL presented improved injection properties. However, the pristine gold electrode on respectively one of the two sides seems to have limited injection yields, leading to the slightly asymmetric shape with respect to the sign of voltage bias. This observation already rules out bare gold contacts on both sides to be optimal.

Next, the results obtained from symmetric devices are presented. Figures 3(a) and 3(b) display the current–density (*J*–*V*) voltage characteristics of symmetric PEDOT:PSS and symmetric MoO_3 single carrier hole only device. In the case of symmetric PEDOT:PSS devices, charge carrier mobilities are independent of annealing temperature up to 200 °C in forward and reverse regimes. However, the device degraded drastically under thermal annealing at 250 °C and current densities (*J*) reduced by two orders of magnitude. Here, the devices are dominated by degradation of injection properties. It can be noticed from the *J*–*V* characteristics that all the devices exhibit a symmetric behavior when the symmetric hole transport materials are used on both sides. This observation is kind of interesting, as

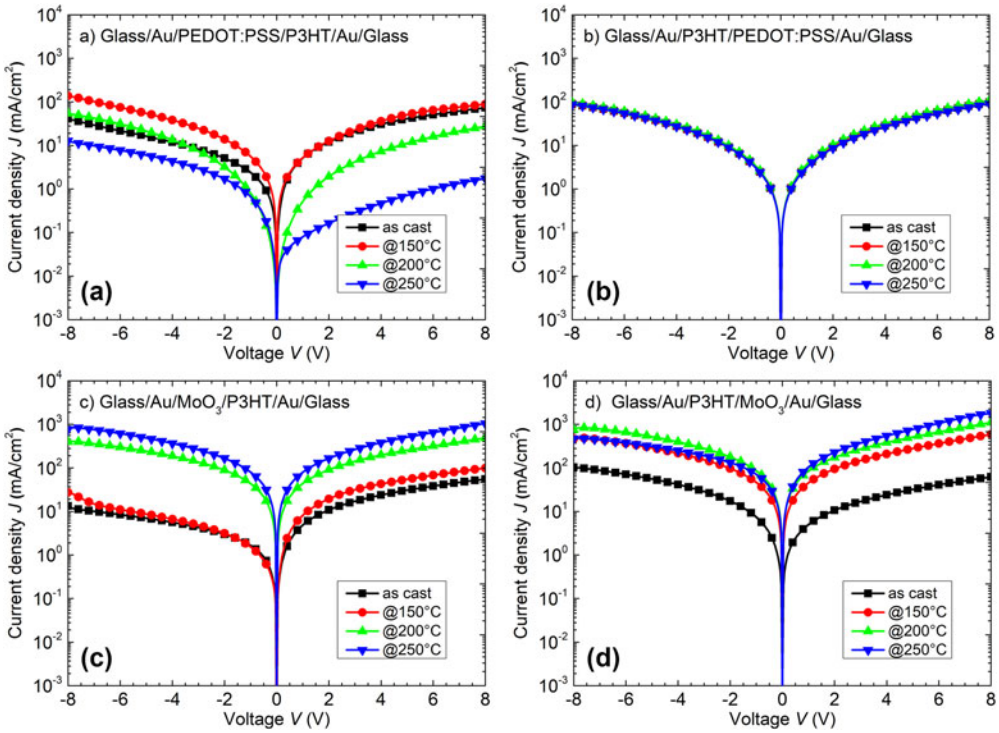


FIG. 2. Diode-characteristics of asymmetric SCLC devices recorded at room temperature and plotted on a semilogarithmic scale. (a) Glass/Au/PEDOT:PSS/P3HT/Au/glass, (b) glass/Au/P3HT/PEDOT:PSS/Au/glass, (c) glass/Au/MoO_3/P3HT/Au/glass, and (d) glass/Au/P3HT/MoO_3/Au/glass.

https://doi.org/10.1557/jmr.2018.203 Published online by Cambridge University Press

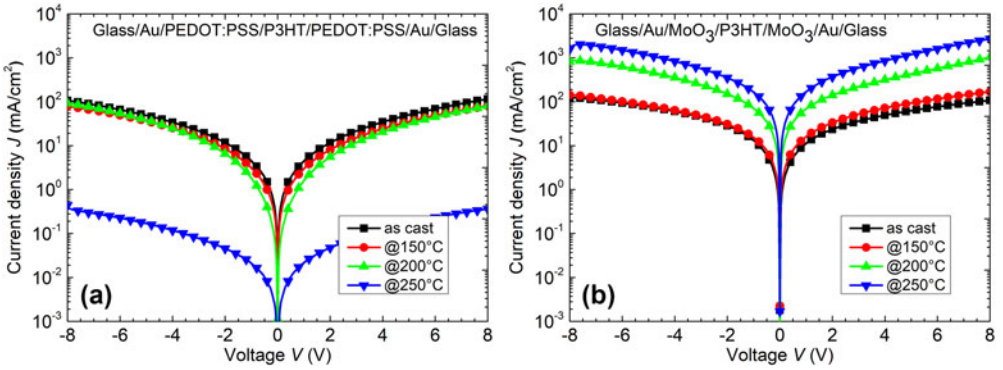


FIG. 3. Diode characteristics of symmetric SCLC devices recorded at room temperature and plotted on a semilogarithmic scale. (a) Glass/Au/PEDOT:PSS/P3HT/PEDOT:PSS/Au/glass and (b) glass/Au/MoO_3/P3HT/MoO_3/Au/glass.

specifically for the asymmetric device exhibiting the Au/P3HT/PEDOT:PSS/Au layer stack, no degradation of current density was observed at 250 °C.

By contrast, the symmetric devices using MoO_3 as HTLs exhibit nicely symmetric *J–V* characteristics. On top of that, a consistent increase of current densities is observed for annealing temperatures above 150 °C, reflecting increased hole mobility due to the improved ordering of the P3HT.[15]

The dark *J–V* curves were fitted with the above-stated Murgatroyd formula [Eq. (1)]. Such SCLC fits for as-cast and melt-crystalized symmetric devices are shown in Fig. 4. Calculated charge carrier mobilities for devices annealed at various temperatures are shown in Fig. 5 and summarized along with the fit-error and the determined built-in voltage in Table II. Although the two interfacial contacts are made from the same electrode, an energy offset of the symmetric devices was found from 100–400 mV, ascribed to differences in the interface between the bottom and top interface. This was essential to correctly interpret the shape of the current–voltage characteristics at low voltage.[25] While for devices using MoO_3, a consistent increase in hole mobility is found, and PEDOT:PSS as HTLs yields the complete opposite behavior. This finding rules PEDOT:PSS out for reliable investigation of thermally treated devices above 150 °C.

It is interesting to mention here that the derived SCLC-mobility of 0.022 cm^2/V s for the melt-crystallized P3HT annealed at 250 °C using MoO_3 as HTL displays, to the best of our knowledge, the highest value reported in the literature for vertical charge transport in P3HT-diodes to date. In other recent studies on disrupted P3HT-films, micropatterning was used to yield vertically oriented P3HT-backbones, and with those even higher vertical charge carrier mobilities of up to ~10 cm^2/V s have been reported.[26–29] The authors showed that those values could be understood as close to the limit since maximum hole mobility values obtained via probing the charge transport only locally by Terahertz spectroscopy[30] yielded one order of magnitude higher mobilities (30–40 cm^2/V s), which coincides with theoretical calculations.[27,31]

In view of that, the herein reported mobility values thus correspond to about one-thousandth of the maximum

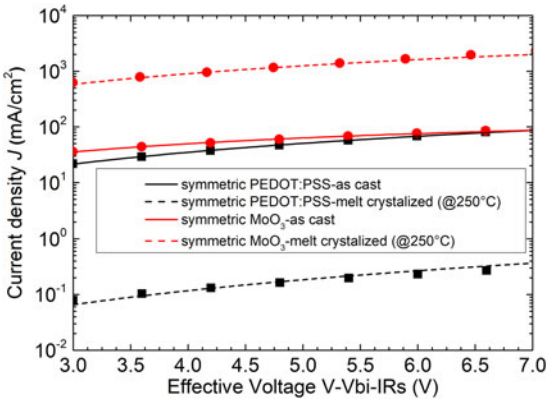


FIG. 4. SCLC fits using Murgatroyd formula and the *J–V* characteristics were corrected for the built-in voltage (V_{bi}) and the voltage drop over the contacts.

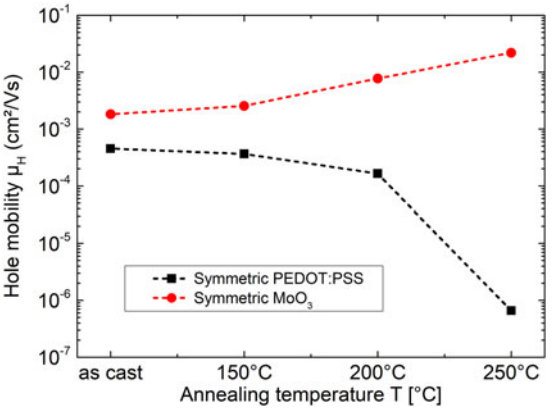


FIG. 5. SCLC hole mobilities obtained from symmetric devices subjected to no (as cast) and annealing at elevated temperatures up to 250 °C. The mobility values were determined by fitting the *J–V* characteristics according to Eq. (1).

https://doi.org/10.1557/jmr.2018.203 Published online by Cambridge University Press

hole mobility in well-ordered P3HT chains along with the backbone. However, our case transport is dominantly following side-chain or π–π stacking direction—in agreement with structural investigations, that either report edge-on or face-on orientation of P3HT crystallites.[32–34] And in either case, this corresponds to a parallel organization of the P3HT-backbones for spin-cast or drop-cast films.[5,6]

To gain deeper insight into possible morphology changes of the HTLs upon annealing, AFM measurements were performed on these HTLs coated on Au electrodes and are shown in Fig. 6. The first observation upon annealing of PEDOT:PSS and MoO_3 films under the same conditions is that there are no dramatic changes. However, there are minor changes observed for the stacks annealed at high temperature. It seems that upon annealing at the most elevated temperature, PEDOT:PSS films develop slightly higher crystallinity, indicated by somewhat increased surface roughness and better visibility of small grainy structures. No apparent changes were observed in case of MoO_3, the apparent increase in grain size should be related to a degradation of the AFM tip itself.

TABLE II. Extracted SCLC hole mobilities obtained from symmetric devices subjected to different thermal annealing conditions up to 250 °C. The mobility values were determined from SCLC fits, and a minimum fitting error occurred for the respective built-in voltage [V_{bi}] reported.

Symmetric device based on HTL	10 min thermal annealing @	Hole mobility (μ_h)/[10^{-3} cm^2/V s]	Minimum fit error χ^2	Built-in voltage V_{bi}/[V]
PEDOT:PSS	As cast	0.453	2.93	0.10
PEDOT:PSS	150 °C	0.364	2.71	0.10
PEDOT:PSS	200 °C	0.164	1.48	0.15
PEDOT:PSS	250 °C	0.00077	2.18	0.40
MoO_3	As cast	1.81	3.68	0.10
MoO_3	150 °C	2.55	3.86	0.15
MoO_3	200 °C	7.73	7.02	0.20
MoO_3	250 °C	21.85	6.84	0.10

To shed further light on possible energetic changes of PEDOT:PSS and MoO_3 films upon annealing, their work function was investigated by KP method, and the results are shown in Fig. 7. For that, four different layer stacks were investigated: (i) glass/gold/PEDOT:PSS (Bottom PEDOT:PSS), (ii) glass/gold/PEDOT:PSS/P3HT/PEDOT:PSS (Top PEDOT:PSS), (iii) glass/gold/MoO_3 (Bottom MoO_3), and (iv) glass/gold/MoO_3/P3HT/MoO_3 (Top MoO_3). Interestingly, the bottom PEDOT:PSS films exhibited almost no variation concerning the work function, while the top PEDOT:PSS films showed a constant drop from close to 5 eV down to about 4.6 eV. More surprisingly, also the bottom MoO_3 exhibited a strong reduction upon annealing from close to 5.2 eV down to slightly below 4.8 eV. However, the top MoO_3 films exhibited the most irregular behavior, initially raised upon annealing from 4.7 eV to about 4.9 eV at 200 °C, then the work function decreased again for temperatures

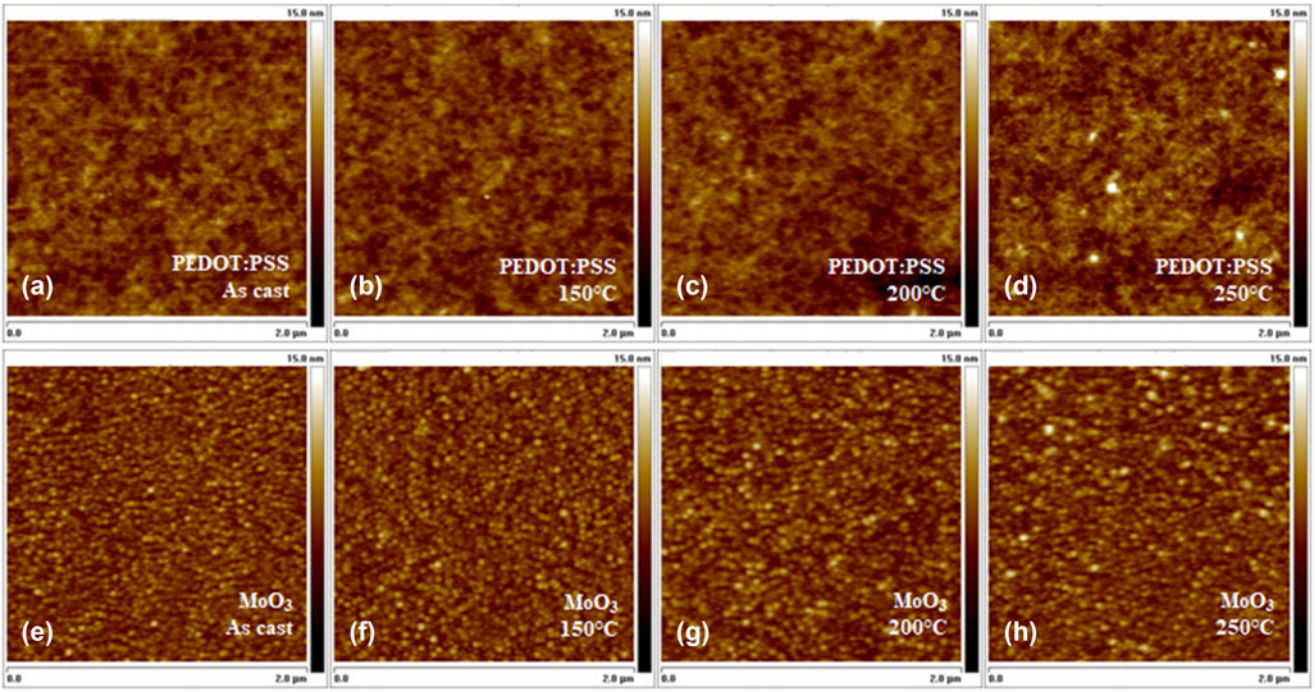


FIG. 6. AFM topography images (2 × 2 μm) showing PEDOT:PSS and MoO_3 films on Au, which have been annealed at 150, 200, and 250 °C. As-cast films are shown as a reference as well. In general, no much change is observed. Upper row: PEDOT:PSS films annealed at (a) as-cast, (b)150 °C, (c) 200 °C, and (d) 250 °C, lower row: MoO_3 films annealed at (e) as-cast, (f) 150 °C, (g) 200 °C, and (h) 250 °C, respectively.

https://doi.org/10.1557/jmr.2018.203 Published online by Cambridge University Press

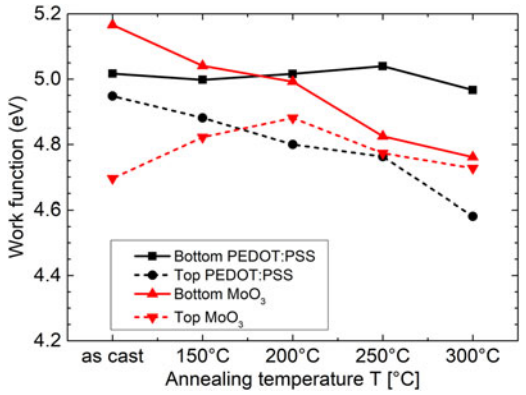


FIG. 7. Work function of bottom and top HTLs (PEDOT:PSS and MoO_3).

up to the maximum investigated here (300 °C). It should be noted here that even though annealing was performed under inert conditions in a glovebox, the KP characterization was performed under air. However, this cannot be the reason for the observed variations in work function. While the work function of PEDOT:PSS depends on the ratio between PSS and PEDOT at the surface,[21,35] not much is known concerning MoO_3. However, the work function of evaporated MoO_3 decreases after exposure to air due to a very thin layer of oxygen-rich adsorbate on the MoO_3 film.[36,37] The work function of MoO_3 can generally be recovered with increasing annealing temperature in vacuum.[36]

It is furthermore clear that the work function for top HTL devices is not the one acting towards the interface to the P3HT layer below. One favorable fact may be that the work function for MoO_3 becomes similar for higher annealing temperatures. However, to understand the full effects, it should be taken into consideration that MoO_3 is known to dope OSCs which results in barrier-free hole injection. Finally, it should be noted that the experimental observation that symmetric single-carrier hole-only devices based on MoO_3 as HTL seem to offer a stable condition concerning favorable contact formation with minimized injection (and thus also extraction) barriers for hole transfer between the electrode and OSCs—here P3HT.

IV. CONCLUSION

With increasing importance of thermal annealing steps—either during semiconductor processing or for testing thermal stability of complete devices based on OSCs such as organic solar cells—the design of stable performing electrodes in combination with charge transport layers becomes essential. Here, we demonstrated that MoO_3 as the HTL could fulfill the expectations for high-temperature stable charge injection and extraction properties. Even though gold was used in this study for the electrodes, also other metals should be yielded stable features, as long as oxidation does not harm contact resistances.

In summary, we presented with gold/MoO_3, a metal electrode/hole transport material combination that can sustain its favorable properties up to annealing temperatures of 250 °C, enabling the study of mobility changes upon melt crystallization of somewhat crystalline regioregular P3HT. To the best of our knowledge, the obtained vertical hole mobility of 0.022 cm^2/V s displays the highest value ever reported to date for pristine P3HT films. It is expected that also other more recent representatives of semicrystalline OSCs can be investigated with respect to their vertical charge transport potential upon melt crystallization.

ACKNOWLEDGMENTS

SA and HH are grateful for financial support from Deutsche Forschungsgemeinschaft (DFG) in the frame of "PhotoGenOrder" project. The authors appreciate for the AFM measurements supported by A. Paszuk at TU-Ilmenau.

REFERENCES

1. P. Friederich, V. Meded, A. Poschlad, T. Neumann, V. Rodin, V. Stehr, F. Symalla, D. Danilov, G. Ludemann, R.F. Fink, I. Kondov, F. von Wrochem, and W. Wenzel: Molecular origin of the charge carrier mobility in small molecule organic semiconductors. *Adv. Funct. Mater.* **26**, 5757 (2016).
2. Y.F. Yao, H.L. Dong, and W.P. Hu: Charge transport in organic and polymeric semiconductors for flexible and stretchable devices. *Adv. Mater.* **28**, 4513 (2016).
3. H. Bassler and A. Kohler: Charge transport in organic semiconductors. In *Unimolecular and Supramolecular Electronics I: Chemistry and Physics Meet at Metal-Molecule Interfaces*, R.M. Metzger, ed. (Springer-Verlag Berlin, Berlin, 2012); p. 1.
4. L.H. Nguyen, H. Hoppe, T. Erb, S. Günes, G. Gobsch, and N.S. Sariciftci: Effects of annealing on the nanomorphology and performance of poly(alkylthiophene): Fullerene bulk-heterojunction solar cells. *Adv. Funct. Mater.* **17**, 1071 (2007).
5. U. Zhokhavets, T. Erb, H. Hoppe, G. Gobsch, and N. Serdar Sariciftci: Effect of annealing of poly(3-hexylthiophene)/fullerene bulk heterojunction composites on structural and optical properties. *Thin Solid Films* **496**, 679 (2006).
6. U. Zhokhavets, G. Gobsch, H. Hoppe, and N.S. Sariciftci: Anisotropic optical properties of thin poly(3-octylthiophene)-films as a function of preparation conditions. *Synth. Met.* **143**, 113 (2004).
7. U. Zhokhavets, G. Gobsch, H. Hoppe, and N.S. Sariciftci: A systematic study of the anisotropic optical properties of thin poly (3-octylthiophene)-films in dependence on growth parameters. *Thin Solid Films* **451–452**, 69 (2004).
8. C. Tanase, E.J. Meijer, P.W. Blom, and D.M. De Leeuw: Unification of the hole transport in polymeric field-effect transistors and light-emitting diodes. *Phys. Rev. Lett.* **91**, 216601 (2003).
9. E.J.W. Crossland, K. Tremel, F. Fischer, K. Rahimi, G. Reiter, U. Steiner, and S. Ludwigs: Anisotropic charge transport in spherulitic poly(3-hexylthiophene) films. *Adv. Mater.* **24**, 839 (2012).

https://doi.org/10.1557/jmr.2018.203 Published online by Cambridge University Press

10. A.J. Mozer, N.S. Sariciftci, A. Pivrikas, R. Österbacka, G. Juška, L. Brassat, and H. Bässler: Charge carrier mobility in regioregular poly(3-hexylthiophene) probed by transient conductivity techniques: A comparative study. *Phys. Rev. B* **71**, 035214 (2005).
11. D. Gebeyehu, B. Maennig, J. Drechsel, K. Leo, and M. Pfeiffer: Bulk-heterojunction photovoltaic devices based on donor–acceptor organic small molecule blends. *Sol. Energy Mater. Sol. Cells* **79**, 81 (2003).
12. C. Kastner, J. Xuechen, D.A.M. Egbe, H. Ade, and H. Hoppe: Correlating domain purity with charge carrier mobility in bulk heterojunction polymer solar cells. *Proc. SPIE* **9184**, 91840Z (2014).
13. A. Diacon, L. Derue, C. Lecourtier, O. Dautel, G. Wantz, and P. Hudhomme: Cross-linkable azido C_{60}-fullerene derivatives for efficient thermal stabilization of polymer bulkheterojunction solar cells. *J. Mater. Chem. C* **2**, 7163 (2014).
14. J. Harnonnet, M. Nakano, K. Nakano, H. Sugino, K. Takimiya, and K. Tajima: Bis(naphthothiophene diimide)indacenodithiophenes as acceptors for organic photovoltaics. *Chem. Mater.* **29**, 9618 (2017).
15. C.R. Singh, G. Gupta, R. Lohwasser, S. Engmann, J. Balko, M. Thelakkat, T. Thurn-Albrecht, and H. Hoppe: Correlation of charge transport with structural order in highly ordered melt-crystallized poly(3-hexylthiophene) thin films. *J. Polym. Sci., Part B: Polym. Phys.* **51**, 943 (2013).
16. N. Boulanger, J.C. Yu, and D.R. Barbero: SWNT nano-engineered networks strongly increase charge transport in P3HT. *Nanoscale* **6**, 11633 (2014).
17. N. Boulanger, V. Yu, M. Hilke, M.F. Toney, and D.R. Barbero: In situ probing of the crystallization kinetics of rr-P3HT on single layer graphene as a function of temperature. *Phys. Chem. Chem. Phys.* **19**, 8496 (2017).
18. Z.P. Kan, L. Colella, E.V. Canesi, A. Vorobiev, V. Skrypnychuk, G. Terraneo, D.R. Barbero, C. Bertarelli, R.C.I. MacKenzie, and P.E. Keivanidis: Charge transport control via polymer polymorph modulation in ternary organic photovoltaic composites. *J. Mater. Chem. A* **4**, 1195 (2016).
19. V. Skrypnychuk, N. Boulanger, V. Yu, M. Hilke, S.C.B. Mannsfeld, M.F. Toney, and D.R. Barbero: Enhanced vertical charge transport in a semiconducting P3HT thin film on single layer graphene. *Adv. Funct. Mater.* **25**, 664 (2015).
20. V. Skrypnychuk, N. Boulanger, V. Yu, M. Hilke, M.F. Toney, and D.R. Barbero: Reduced crystallinity and enhanced charge transport by melt annealing of an organic semiconductor on single layer graphene. *J. Mater. Chem. C* **4**, 4143 (2016).
21. O. Synooka, F. Kretschmer, M.D. Hager, M. Himmerlich, S. Krischok, D. Gehrig, F. Laquai, U.S. Schubert, G. Gobsch, and H. Hoppe: Modification of the active layer/PEDOT:PSS interface by solvent additives resulting in improvement of the performance of organic solar cells. *ACS Appl. Mater. Interfaces* **6**, 11068 (2014).
22. Y.Z. Guo and J. Robertson: Origin of the high work function and high conductivity of MoO_3. *Appl. Phys. Lett.* **105**, 222110 (2014).
23. P. Murgatroyd: Theory of space-charge-limited current enhanced by Frenkel effect. *J. Phys. D: Appl. Phys.* **3**, 151 (1970).
24. F. Herrmann, B. Muhsin, C.R. Singh, S. Shokhovets, G. Gobsch, H. Hoppe, and M. Presselt: Influence of interface doping on charge-carrier mobilities and sub-band gap absorption in organic solar cells. *J. Phys. Chem. C* **119**, 9036 (2015).
25. A.S.J. Dacuña: Modeling space-charge limited currents in organic semiconductors: Extracting trap density and mobility. *Phys. Rev. B* **84**, 195209.
26. H.W. Ro, B. Akgun, B.T. O'Connor, M. Hammond, R.J. Kline, C.R. Snyder, S.K. Satija, A.L. Ayzner, M.F. Toney, C.L. Soles, and D.M. DeLongchamp: Poly(3-hexylthiophene) and [6,6]-phenyl-C_{61}-butyric acid methyl ester mixing in organic solar cells. *Macromolecules* **45**, 6587 (2012).
27. V. Skrypnychuk, G. Wetzelaer, P.I. Gordiichuk, S.C.B. Mannsfeld, A. Herrmann, M.F. Toney, and D.R. Barbero: Ultrahigh mobility in an organic semiconductor by vertical chain alignment. *Adv. Mater.* **28**, 2359 (2016).
28. G. Wang, J. Swensen, D. Moses, and A.J. Heeger: Increased mobility from regioregular poly(3-hexylthiophene) field-effect transistors. *J. Appl. Phys.* **93**, 6137 (2003).
29. K.J. Baeg, D. Khim, D.Y. Kim, J.B. Koo, I.K. You, W.S. Choi, and Y.Y. Noh: High mobility top-gated poly(3-hexylthiophene) field-effect transistors with high work-function Pt electrodes. *Thin Solid Films* **518**, 4024 (2010).
30. P.D. Cunningham and L.M. Hayden: Carrier dynamics resulting from above and below gap excitation of P3HT and P3HT/PCBM investigated by optical-pump terahertz-probe spectroscopy. *J. Phys. Chem. C* **112**, 7928 (2008).
31. J.E. Northrup: Atomic and electronic structure of polymer organic semiconductors: P3HT, PQT, and PBTTT. *Phys. Rev. B* **76**, 245202 (2007).
32. R.J. Kline, M.D. McGehee, E.N. Kadnikova, J.S. Liu, J.M.J. Frechet, and M.F. Toney: Dependence of regioregular poly(3-hexylthiophene) film morphology and field-effect mobility on molecular weight. *Macromolecules* **38**, 3312 (2005).
33. R. Noriega, J. Rivnay, K. Vandewal, F.P.V. Koch, N. Stingelin, P. Smith, M.F. Toney, and A. Salleo: A general relationship between disorder, aggregation and charge transport in conjugated polymers. *Nat. Mater.* **12**, 1038 (2013).
34. J. Balko, G. Portale, R.H. Lohwasser, M. Thelakkat, and T. Thurn-Albrecht: Surface induced orientation and vertically layered morphology in thin films of poly(3-hexylthiophene) crystallized from the melt. *J. Mater. Res.* **32**, 1957 (2017).
35. S. Nau, N. Schulte, S. Winkler, J. Frisch, A. Vollmer, N. Koch, S. Sax, and E.J. List: Highly efficient color-stable deep-blue multilayer PLEDs: Preventing PEDOT:PSS-induced interface degradation. *Adv. Mater.* **25**, 4420 (2013).
36. I. Irfan, A. James Turinske, Z. Bao, and Y. Gao: Work function recovery of air exposed molybdenum oxide thin films. *Appl. Phys. Lett.* **101**, 093305 (2012).
37. P. Schulz, J.O. Tiepelt, J.A. Christians, I. Levine, E. Edri, E.M. Sanehira, G. Hodes, D. Cahen, and A. Kahn: High-work-function molybdenum oxide hole extraction contacts in hybrid organic–inorganic perovskite solar cells. *ACS Appl. Mater. Interfaces* **8**, 31491 (2016).

https://doi.org/10.1557/jmr.2018.203 Published online by Cambridge University Press